


## Homogeneous and inhomogeneous line shape of the electronic excitation of a single molecule on a surface

Christian Marquardt, Alexander Paulheim, Manuel Hochheim, Thomas Bredow, and Moritz Sokolowski  
*Universität Bonn, Institut für Physikalische und Theoretische Chemie, Wegelerstr. 12, 53115 Bonn, Germany*

 (Received 6 March 2020; revised 27 May 2021; accepted 2 June 2021; published 16 July 2021)

The homogeneous line profile of a single molecule adsorbed on a surface was measured by high resolution laser spectroscopy. For the prototype organic molecule 3,4,9,10-perylene tetracarboxylic dianhydride (PTCDA) adsorbed at step sites of a thin epitaxial film of KCl on Ag(100) we measure a zero phonon line of Lorentzian shape with a full width at half maximum of  $460 \pm 25$  MHz at a temperature of 6 K. The line is considerably narrower than those which have been recorded in fluorescence spectra of this and similar single molecules that were excited under the tip of a scanning tunneling microscope. The related time is, however, by a factor of  $\sim 15$  smaller than the lifetime of PTCDA recorded in liquid He droplets, likely due to thermal dephasing. From this knowledge on the single molecule line profile, we also explain the inhomogeneous line profile of an ensemble of PTCDA molecules by a quantitative model based on surface defects.

DOI: [10.1103/PhysRevB.104.045415](https://doi.org/10.1103/PhysRevB.104.045415)

### I. INTRODUCTION

Probing the properties of single molecules is of great interest for the understanding of interactions and processes on the microscopic scale. Optical single molecule detection was first performed on molecules in solid hosts [1–6]. Using high spatial and/or spectral dilution one achieves access to the homogeneous line profile of a single molecule. It exhibits a width that is typically several orders of magnitude smaller than the width of the inhomogeneous line profile of an ensemble of molecules which are subject to statistical interactions with their local environment [2]. Hence, single molecule spectra can be used to probe interactions [7], site specific processes, or smallest environmental changes of molecules with highest resolution.

One intrinsic difficulty of experiments performed on single molecules embedded in three-dimensional host materials is the limited control of the microscopic structural properties of the probed molecules. Therefore, optical single molecule experiments at surfaces which take advantage of the spatial resolution of scanning tunneling microscopy (STM) have attracted great interest [8–13]. For appropriate molecules that are deposited on thin insulating films it is possible to image the molecular adsorption complex by STM and to record in parallel the light emitted by the molecules when these are excited by inelastic tunneling of electrons between the tip and the surface (STM-LE). Recently, these experiments have been subject to great progress as, for instance, spectra showing coupling to molecular vibrational modes were obtained [8–10].

One aspect among others that is not sufficiently understood so far concerns the shape and, in particular, the width of the spectral emission line in STM-LE experiments. Compared to the linewidth of optical transitions achieved by high resolution optical single molecule spectroscopy in solids, which range between 10 [2] and a few hundreds MHz [6], the narrowest line reported from STM-LE experiments that we

know of is 600 GHz in width [12]. This value is already small for a typical photoluminescence experiment performed on an ensemble of molecules, but still orders of magnitude larger than the linewidth expected for the emission spectrum from a single molecule. Moreover, in many STM-LE experiments rather large linewidths on the order of a few terahertz were achieved [8–10], and up to now it is not understood which mechanisms cause this line broadening. One possibility could be that it is an intrinsic property of the molecules related to their adsorption on the surface which leads to a reduced lifetime of the excitation. Alternatively, the currently debated excitation and emission processes under the STM tip which involve a tip plasmon are responsible [14,15]. Hence, the situation calls for an independent determination of the line profile of a single molecule adsorbed on a surface by laser spectroscopy.

Here we report single molecule spectra of 3,4,9,10-perylenetetracarboxylic dianhydride (PTCDA) molecules adsorbed at step sites of the (100) surface of KCl. For PTCDA molecules on a three-monolayer-thick film of NaCl, Kimura *et al.* recently published a line profile of the STM induced fluorescence (FL) with a full width at half maximum (FWHM) of  $41 \text{ cm}^{-1}$  at a sample temperature of  $\sim 6$  K [16]. The probed system is thus very similar to ours and allows comparison. Helpfully, the structural and optical properties of PTCDA on KCl(100) are rather well understood [17–21]. After deposition at low temperatures, mild annealing induces an irreversible migration of the molecules to monoatomic KCl step edges which remain from the KCl growth process [19]. The interaction of the molecules and KCl ion pairs causes the formation of local step edge vacancies which are partially occupied by the molecule. Different types of these adsorption sites of PTCDA at steps exist and have been described in detail [17,20]. They can be discerned in optical spectra from slightly different transition energies [20]. In the present experiment, two adsorption sites which are energetically favored

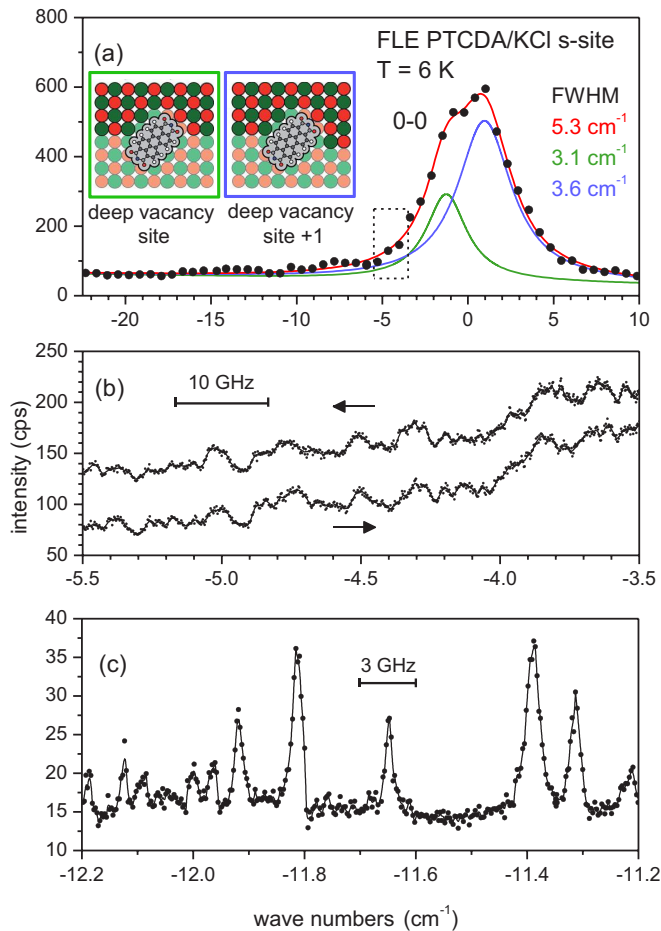


FIG. 1. Fluorescence excitation spectra of PTCDA molecules adsorbed at KCl step sites measured at 6 K. (a) Low resolution scan of the inhomogeneously broadened 0-0 transition. The spectrum was measured by scanning the thin etalon of the ring laser in steps of  $0.63 \text{ cm}^{-1}$  (defined by the free spectral range of the thick etalon). The profile is fitted by a sum (red) of two Lorentzian profiles related to two contributing adsorption sites (green/blue). Real space models of these sites are given in the inset. (b) Two consecutive high resolution scans in the low energy wing of the inhomogeneously broadened profile. The region of the scan is marked in panel (a) by the dashed box. The scans show the statistical fine structure. Only minor changes are observed between the two scans. In panels (a) and (b) the density of the molecules was about  $10^{-4}$  ML, and the laser intensity was  $15 \text{ W/cm}^2$ . (c) High resolution scan of a scan region further displaced from the center of the profile ( $-11 \text{ cm}^{-1}$ ), showing single zero-phonon lines of single molecules. For this scan, the density of the molecules was reduced to about  $10^{-6}$  ML and the laser intensity was  $300 \text{ mW/cm}^2$ .

contribute. Both are about equally occupied because they exhibit similar formation energies [17]. The inset of Fig. 1(a) shows models of the arrangement of the  $\text{K}^+$  and  $\text{Cl}^-$  ions around the PTCDA molecules at these step sites. The models were derived from STM data and density functional theory (DFT) [21]. Notably, Coulombic interactions with the surface ions cause a significant out-of-plane distortion of the PTCDA molecule with respect to its planar gas phase geometry, e.g., the carboxylic O atoms are displaced up to  $0.4 \text{ \AA}$  below the

backbone. We deliberately used the adsorption at the step sites instead of the terraces sites because these are better suited for the time demanding single molecule experiments due to their higher thermal stability.

Besides the knowledge of the single molecule spectra, the detailed understanding of the inhomogeneously broadened spectra of the ensemble is of principle interest, too, as these provide statistically averaged information on the molecular environment. Here we use the information of a deltalike single molecule line shape to quantitatively describe and analyze the inhomogeneous line profile. As we describe in detail below, the shape and width of the inhomogeneous line profile yields information on the defect concentration of the KCl film in the environment of the probed molecules.

## II. EXPERIMENT

### A. KCl film growth and deposition of PTCDA

The experiments were performed under ultrahigh vacuum (UHV). As a model for the KCl(100) surface we used KCl films that were epitaxially grown on a Ag(100) single crystal surface. The preparation of the KCl films is described in detail in [22]. The advantage of the epitaxial films over KCl bulk samples is given by the good thermal coupling via the Ag substrate. Our films had a typical thickness of ten atomic layers making interfacial effects from the underlying Ag(100) surface negligible [23]. The sample was cooled by liquid He and the lowest accessible temperature was 6 K [24].

The PTCDA was sublimed onto the sample from a homemade Knudsen-type evaporator. The PTCDA flux was monitored by a quadrupole mass spectrometer (QMS) operated at  $m/z = 392$  amu. We specify the surface coverage of PTCDA in monolayers (ML). Hereby, 1 ML refers to a coverage of  $7.5 \times 10^{-3}$  molecules per  $\text{\AA}^2$  and corresponds to a compact layer of flat-lying PTCDA molecules [22]. For preparing samples with ultralow coverages for the present experiments, very low and ultralow densities of  $10^{-4}$  and  $10^{-6}$  ML the temperature of the evaporator was lowered such that the flux was at the detection limit of the QMS, i.e.,  $1.5 \times 10^{-4}$  ML/min. Typical temperatures of the PTCDA crucible were between 600 and 630 K. The sample was held at 20 K during deposition. For a deposition time of  $\approx 1$  s we estimate a maximal coverage of  $\approx 2 \times 10^{-6}$  ML. This corresponds to about one molecule per  $\mu\text{m}^2$ . Directly after the deposition at 20 K the molecules are statistically adsorbed on the KCl terraces. Hence the sample was heated to 150 K for 20 min in order to thermally induce a migration of all PTCDA molecules to monoatomic step edges of the KCl(100) surface [19]. Scanning tunneling microscopy images demonstrating the adsorption scenario at the KCl step sites can be found in [17].

### B. Optical spectroscopy

Below we report FL excitation (FLE) spectra which were recorded under excitation by a cw ring laser with a very narrow bandwidth, which safeguarded negligible experimental broadening. For these experiments the sample was cooled to 6 K and transferred into a glass head standing out at the end of the UHV chamber. The glass head and the whole detection

apparatus were placed inside a black box for an exclusion of room light. In a first step, the quality of the sample was checked by FL spectroscopy [19]. Here, the molecules were excited by an optically pumped semiconductor laser (Coherent Sapphire LP USB CDRH) operated at 458.0 nm (50 mW). For FLE spectroscopy we used a tunable ring laser (Sirah Matisse II DS) operated with Coumarin 498 as the laser dye. The ring laser was pumped by an optically pumped semiconductor laser (Coherent Genesis CX 480 4000) at 480 nm and 4 W excitation power. With a customized output coupler, stable and tunable single mode operation with a laser output  $> 50$  mW was obtained between 495 and 525 nm. The wavelength of the laser was monitored with a wavelength meter (HighFinesse Angstrom WS/6).

The excitation light was filtered by a 510 nm short pass filter in order to block unwanted fluorescence from the laser dye. Subsequently, the laser beam was focused onto the sample. We focused the laser under an angle of incidence of  $45^\circ$  with respect to the sample surface. The directly reflected beam was blocked by a beam dump. The size of the focused spot on the sample was approximately 0.2 mm in diameter. The number of molecules inside the focus was estimated to be 40 000 for a coverage of  $10^{-6}$  ML. We used different power densities between  $\approx 30$  and  $1500$  mW/cm<sup>2</sup> for excitation. To reduce the laser power, neutral density filters were used. The fluorescence from the sample was collected and focused on the entrance slit of a spectrograph by a pair of collecting lenses ( $f_1 = 100$  mm,  $NA_1 = 0.22$ ,  $f_2 = 200$  mm). The excitation light scattered from the sample was blocked by a 520 nm long pass filter. The spectrograph (Acton 2300i,  $f/\# = 4$ ,  $f = 0.3$  m) was equipped with a liquid nitrogen cooled CCD camera [Spec10:100BR(LN)]. We used a wide-open entrance slit (2 mm) for increased detection efficiency and hardware binning of the CCD pixels (binning of each 20 pixel columns) to minimize readout noise.

The FLE spectra were computed from FL spectra recorded for varying excitation wavelength by integration of the FL intensity in the regime between 518 and 602 nm. Each FL spectrum was measured with an exposure time of 2 s, while continuously scanning the cavity of the ring laser with a speed of 30 MHz/s. The instrumental broadening of the FLE spectra is determined by the width of the laser line of the ring laser. We operated the laser in the nonfrequency stabilized mode with a linewidth of  $< 20$  MHz rms. For this experimental setup we estimate an overall detection efficiency of 0.3% of the emitted photons. This value is comparably low, which is also the reason for the so far comparably high but necessary exposure time. The detection efficiency is majorly limited by the NA (0.22) of the collection optics. Therefore, currently only 2.5% of all emitted photons are collected. Further losses are due to the recorded and evaluated spectral range of the FL spectrum (35% efficiency), the spectrograph ( $\approx 65\%$ ), the efficiency of the CDD camera ( $\approx 65\%$ ), and partial reflections on the surfaces of lenses and filters ( $\approx 80\%$ ).

### III. RESULTS AND DISCUSSION

Figure 1(a) displays the inhomogeneously broadened FLE profile of the pure electronic  $S_0/S_1$  transition (0-0 transition). The FWHM of the profile amounts to  $5.3$  cm<sup>-1</sup> ( $\approx 160$  GHz);

the center of the profile is located at  $20\,140.5$  cm<sup>-1</sup>. The profile and, in particular, the small indentation at its maximum, can be well fitted by a superposition of two Lorentzian profiles, separated in energy by  $2$  cm<sup>-1</sup>. They represent inhomogeneous line profiles related to the two adsorption sites shown in the inset. This assignment was derived on the basis of DFT calculations [20].

#### A. Position and shape of the inhomogeneous line profile

The central wavelength of the inhomogeneous broadening is shifted by  $\approx 10$  cm<sup>-1</sup> compared to the position reported in our earlier publications [19,20]. This deviation is due to the different method of determination. While the wavelength of the excitation laser in earlier experiments was determined via a manually calibrated spectrometer, for the present experiment a self-calibrated wavelength meter with higher absolute accuracy was used. This energy is slightly larger than the value obtained in Ref. [19], but within the range of FWHM values obtained for typical preparations.

Generally, inhomogeneously broadened line profiles are expected to exhibit Gaussian shapes that originate from corresponding distributions of the energies of superposing homogeneous lines [25]. However, fitting the profile in Fig. 1(a) by two Gaussians was not successful. This is demonstrated in Fig. 5(c) below. As said, the profile could be well fitted by two Lorentzians, instead. The same result was already obtained for the inhomogeneous line profile of PTCDAs molecules adsorbed at NaCl step sites [20]. The origin of this Lorentzian line shape was unclear so far. As we will explain below, it originates from electrostatic dipole-dipole coupling with statistically distributed structural defects of the KCl surface.

In addition to long scans of the complete profile, short scans with high resolution were measured on the low energy wing of the profile. Such a scan is shown in Fig. 1(b). The scan region comprises an energy range located on the low energy side of both transitions contributing to the profile [Fig. 1(a)]. The intensity exhibits distinct local maxima and minima. With very few exceptions these features do not change under repeated scanning as demonstrated in Fig. 1(b). We explain them by the so-called statistical fine structure, known from spectra of single molecules in solid hosts [25]. The fine structure resembles the distribution of molecular transition energies inside the excitation area of the laser on the sample that lead to distinct zero-phonon lines (ZPLs) of the individual molecules. From the appearance and the width of the local maxima in the statistical fine structure seen in Fig. 1(b) we derive that the linewidth of single molecules is by orders of magnitude smaller than that of the inhomogeneous broadened line. However, due to the superposition of signals from many molecules it was not possible to measure the ZPL of single molecules under these experimental conditions.

#### B. Single molecule spectroscopy

Therefore, we recorded spectra of a smaller number of molecules. This was achieved by scanning energy regions further off the center of the inhomogeneously broadened profile ( $-11$  cm<sup>-1</sup>). In parallel, we reduced the density of the molecules on the surface and hence the number of molecules

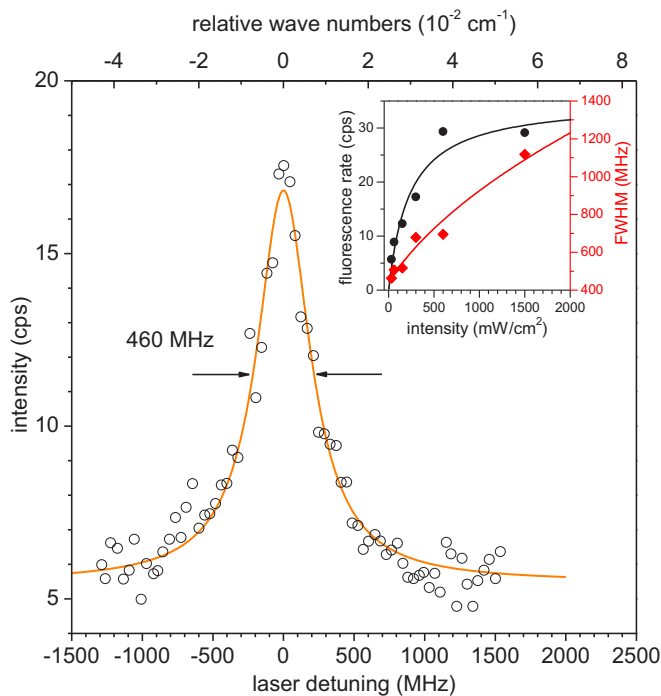


FIG. 2. FLE profile of a single PTCDA molecule located at a step site of the KCl(100) surface. The profile was measured at a laser intensity of  $30 \text{ mW/cm}^2$  and a temperature of 6 K. The red line is a fit by a Lorentzian with a FWHM of 460 MHz. The inset shows the saturation behavior and power broadening of single molecule peaks. Due to experimental reasons the maximum FL rate (black dots) and linewidth (red diamonds) were evaluated for different molecules. The solid lines are fits to the data points according to the saturation behavior of a molecular three-level system. For further details see text.

within the excitation area of the laser spot by a factor of  $\sim 100$ . Figure 1(c) shows such a scan. There, isolated peaks on a smooth baseline with no additional substructure can be observed. As expected, the spectral density of the peaks decreased. The observed peaks correspond to the ZPL of individual molecules.

A scan of a single ZPL is shown in Fig. 2. The fit demonstrates that the ZPL exhibits a Lorentzian shape, which is expected for a homogeneous line profile [2]. The same line profile was seen for other ZPLs. The smallest linewidth (FWHM) which we achieved was  $\Delta\nu = 460 \pm 25 \text{ MHz}$  (i.e.,  $0.0153 \text{ cm}^{-1}$ ). It was measured at the lowest accessible temperature of 6 K and a small laser intensity of  $30 \text{ mW/cm}^2$ . These experimental conditions minimize line broadening by temperature or saturation of the transition (see below). This linewidth is considerably smaller (a factor of  $\sim 2500$ ) compared to that of  $41 \text{ cm}^{-1}$  which has been measured for single PTCDA molecules on a film of three monolayers of NaCl on Ag(111) by STM-LE [16]. The linewidth we obtain is, however, significantly larger than those linewidths that were typically measured in other optical single molecule experiments [3,5,26].

The width of homogeneous profiles is given by the reciprocal dephasing time ( $\Delta\nu = 1/\pi T_2$ ) which comprises the FL lifetime  $T_1$  and the pure dephasing time  $T_2^*$ :  $\Delta\nu = 1/2\pi T_1 +$

$1/\pi T_2^*$  [26]. Bünermann measured a FL lifetime of 5.5 ns from time resolved FL of isolated PTCDA molecules dissolved in ultracold He droplets [27]. We take this value as a lower limit for the lifetime  $T_1$  of the isolated molecule. It is by a factor of 7.9 larger than the dephasing time  $T_2 = 0.70 \text{ ns}$  calculated from our linewidth. Thus, interactions with phonons and local librations related to the molecular environment cause a relevant thermal dephasing time  $T_2^*$  [26], and/or, in addition, structural and electronic distortions of the molecule [21], related to the adsorption process on the surface effect  $T_1$ . At present, we cannot disentangle the two contributions. Because our lowest achievable temperature was limited to 6 K, and on the basis of trends derived from spectra measured at very low temperatures (1.5 K) [2,3,6]), we tentatively assign the broadening to thermal dephasing. However, importantly, our data limit the lifetime reduction with respect to Bünermann's value from molecular distortions due to adsorption to  $T_1 = 0.35 \text{ ns}$ . Hence, the lifetime is not reduced by a factor larger than 15.

The single molecule nature of the line is also verified by the saturation of the FL intensity [3,28] and the broadening of the profile [3] for increasing laser intensity (LI). The respective experimental data are shown in the inset of Fig. 2. Both data sets agree within the uncertainties of the experiment with the expected behavior. Importantly, extrapolating the LI to zero yields a minimal linewidth of  $443 \pm 33 \text{ MHz}$ . This ensures that significant power broadening can be excluded at the low LI used for recording the profile in Fig. 2.

### C. Power density dependence of the line profile

We report experimental details concerning the analysis of the power broadening and saturation of the FL intensity that are reported in the inset of Fig. 2. For studying the saturation behavior of the molecular transitions, i.e., the dependency of the profile height and width on the laser intensity, we varied the laser intensity between 30 and  $1600 \text{ mW/cm}^2$ . The accessible range was limited by the detection efficiency for the lowest intensity and by the signal to background ratio for the highest intensity. The measured peaks were evaluated by subtracting a constant background signal and fitting the profile with a Lorentzian. Then the FL rates at the peak maximum and the FWHM of the Lorentzian fit were extracted. We note that unlike previous single molecule studies [6,29], the plotted data points correspond to different molecules. This was necessary since we did not succeed in measuring the complete intensity range for one single molecule, which was mainly due to the noted instabilities of the ZPL upon excitation. Due to the defined adsorption geometry of the molecules on the sample (the molecules adsorb planar with two possible orientations rotated by  $90^\circ$  with respect to each other) an uncertainty in the orientation of the molecules with respect to the polarization of the laser can be excluded by the selective excitation of one of the two orientations [19]. However, due to the different positions of the molecules inside the Gaussian intensity distribution of the laser, the error bars on the intensity axis are large. Nevertheless, the obtained data set still allows observing the general trends and estimating the system parameters.

The FL rate (inset of Fig. 2, black data) shows a monotone rise and a saturation behavior that is typical for single

molecules and can be described by the model of a molecular three-level system with a triplet bottleneck [3,28]

$$R = R_{\infty} \frac{I/I_S}{1 + I/I_S},$$

where  $R$  is the FL rate obtained at a power density  $I$  of the laser, with the maximum FL rate  $R_{\infty}$  and the saturation intensity  $I_S$ . By fitting the data to the model we determined an experimental maximum FL rate  $R_{\infty}$  of  $35 \pm 4$  cps and a saturation intensity  $I_S$  of  $230 \pm 80$  mW/cm<sup>2</sup>.

Within the same model also the saturation broadening (inset of Fig. 2, red data) can be described. Here, the width of the profile  $\Delta\nu$  increases with the root of the laser intensity as can be seen from [3]

$$\Delta\nu = \Delta\nu_0 \sqrt{1 + I/I_S},$$

where  $\Delta\nu_0$  is the width of the profile at vanishing laser intensity. The saturation intensity  $I_S$  obtained from the fit was  $300 \pm 70$  mW/cm<sup>2</sup>. This is larger but within the error bar of the value obtained from the saturation of the FL rate. For the minimal linewidth a value of  $443 \pm 33$  MHz is obtained, which means that a significant saturation broadening can be excluded at the lowest applicable laser intensity.

For a comparison with other experiments, the experimental maximum FL rate  $R_{\infty}$  has to be corrected for the detection efficiency of the experimental setup, namely, by 0.3% (see above). After correction a maximum FL rate  $R_{\infty} \approx 11\,500$  photons per second is obtained, which is comparable to experiments on terrylene in hexadecane [29]. Also the obtained saturation intensity is in the typical range [28].

Also typical for single molecule spectra are shifts or even vanishing of ZPLs, if these are scanned repeatedly. This spectral diffusion strongly depends on the LI and are seen here, too. While for the lowest LI, i.e., up to 60 mW/cm<sup>2</sup>, barely any spectral shifts were observed, for higher LI ( $> 150$  mW/cm<sup>2</sup>), however, the probability is significant. Hence, the shifts are due to photophysical processes that are induced by the energy provided by the excitation of vibrational modes in the FL process. Structural modifications, e.g., displacements of KCl ion pairs in the further environment of the molecule, are most likely responsible.

A scan illustrating an instable ZPL is shown in Fig. 3(a). An abrupt and irreversible drop in the intensity to the background level is observed when the laser is scanned into the wing of the ZPL. This is most likely explained by a larger spectral shift of the ZPL to a position outside the scan range. A typical scan of a rarely found metastable ZPL is shown in Fig. 3(b). The ZPL undergoes small jumps (often  $< 1$  GHz) so that the ZPL appears at a different position inside the scan range. The probability for these small spectral shifts is increased at resonance with the laser. For example, the ZPL in Fig. 3(b) is shifted by  $\approx 500$  MHz to lower energies when the laser is approaching the resonance. However, also nonphotophysical, likely thermally induced, shifts of the ZPL were observed. This is seen in the last scan in Fig. 3(b). A small intensity drop at the position of the maximum in the first scan is observed. This can only be explained by a back-shifting of the ZPL from the position in the third scan to the start position (seen in the first scan) during the time the laser was not in resonance with the ZPL.

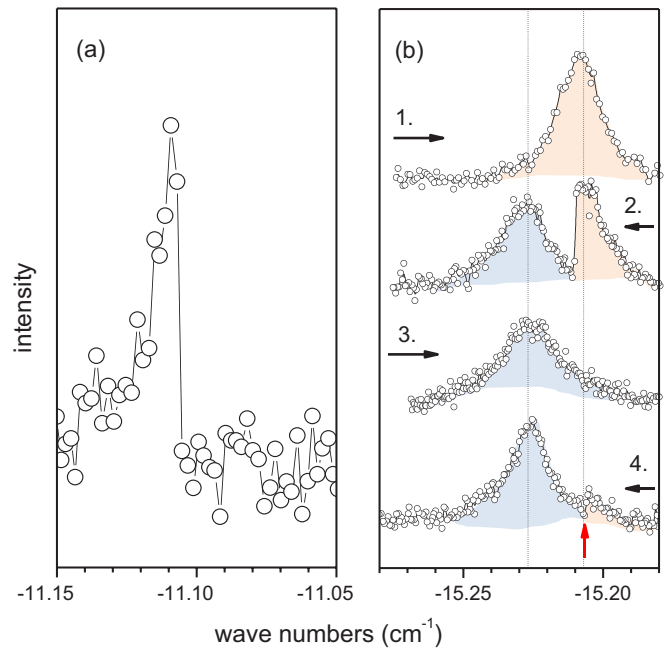


FIG. 3. Vanishing and shifting of the ZPL due to spectral jumps. (a) Laser induced vanishing of an instable ZPL. The intensity drops to the baseline intensity while scanning the wing of the ZPL. The laser intensity was 250 mW/cm<sup>2</sup>. (b) Sequence of four consecutive scans of a metastable ZPL (top to bottom). The scan directions are marked by black arrows. The ZPL is stable during the first scan (top); it is subject to a laser induced shift of  $\approx 500$  MHz to lower energy during the second scan. During the third scan, it is stable again. During the fourth scan, a minimal intensity drop at the position of the ZPL in the first scan is noted (red arrow) that indicates a back-shift of the ZPL to the starting position between the third and fourth scan. Laser intensity: 300 mW/cm<sup>2</sup>.

#### D. Inhomogeneously broadened spectra

We come back to the explanation of the inhomogeneous line profile of an ensemble of molecules [Fig. 1(a)]. Obviously, it results from the superposition of many ZPL that are statistically shifted in their positions due to variations in the environment of the molecules. Because the ZPL are smaller by a factor of about 200 than the inhomogeneous line profile, the contributing ZPL can be considered as  $\delta$ -like peaks on this scale. Hence, the inhomogeneous line profile resembles the distribution of the transition energies. In the present example, the energetic shifts are due to structural variations in the KCl substrate, namely, deviations of the step edges hosting the PTCDA adsorption sites from ideal straight steps in the further vicinity of the adsorption site of the molecule. Relevant are kinks of the steps or additional/missing KCl dipoles. Such defects are observed in STM images [17]. These defects have an impact on the transition energy due to long range Coulomb interactions between the charges of the additional/missing K<sup>+</sup> and Cl<sup>-</sup> ions and the partial charges on the PTCDA molecule. The distribution and size of the partial charges on the molecule in the ground state ( $S_0$ ) and the excited state ( $S_1$ ) depends on its adsorption site and the resulting electronic and structural details.

Evidently, a stochastic approach is needed to describe the distribution of transition energies [30]. In our case, the interaction of a dipole on the molecule ( $\vec{p}_m$ ) with a statistical field of dipoles related to KCl ion pairs yields the simplest but successful model. Kador has used the stochastic approach [30] to explain the optical line profiles of molecules embedded in three-dimensional matrices [31]. He verified that dipole-dipole interactions lead to Lorentzian profiles in the limit of low defect concentrations. Apparently, this situation is met here, too. However, since the surface is mainly a two-dimensional system, some modifications in the theory arise which we describe in detail below. For a quantitative estimation of the defect concentration from the linewidth we have used a value of  $|\Delta\vec{p}_m| = 1.5$  D for the change in the dipole of the PTCDA upon the  $S_0/S_1$  transition and an averaged FWHM of  $\approx 3$  cm<sup>-1</sup> of the respective line profiles related to the two adsorption sites. These values yield a defect concentration of  $\approx 0.6 \times 10^{-2}$ , meaning that we have one structural defect per 150 KCl ion pairs, which appears reasonable. We describe the details of this analysis in the following.

### E. Stochastic approach

The line shapes of inhomogeneously broadened spectra can be calculated according to the stochastic theory described by Stoneham [30]. It was applied to optical transitions of molecules embedded in matrices by Kador [31]. The theory assumes the presence of uncorrelated defects in the environment of the absorbing/emitting molecule. More elaborate approaches which include spatial correlations of the defects are also available [32]. Here we limit ourselves to the case of uncorrelated defects, because this is sufficient to capture the relevant physics.

The central core of the theory is given by pairwise interactions of the ground ( $S_0$ ) and the excited state ( $S_1$ ) of a molecule with many distributed defects (perturbers) in the environment of the molecule. The interactions of the defects and the molecule superpose and cause a differential energetic shift of the transition energy with respect to the unperturbed transition energy ( $\nu_0$ ) of the molecule in a defect-free environment. Statistical variations in the spatial distribution and the orientation of the defects in the environment of a molecule cause different shifts of the respective transition energies leading to perturbed spectra. The inhomogeneous line shape is thus given by the superposition of the perturbed spectra of many molecules. The individual perturbed spectra are given by the zero-phonon lines at different energies that were described above.

In our case, the unperturbed transition energy corresponds to the transition energy of a molecule located at a perfectly straight and infinitely long step edge of the KCl substrate separating two structurally perfect terraces. It is given by the difference of the adsorption energies of the  $S_1$  and  $S_0$  states, i.e., in wave numbers we have

$$\nu_0 = \frac{1}{hc}[E(S_1) - E(S_0)], \quad (1)$$

where  $h$  denotes Planck's constant and  $c$  the velocity of light. As said, both the  $S_1$  and the  $S_0$  state are subject to interactions with defects. In the present situation, the generic entity for the description of these defects is additional or missing (vacancy)

KCl ion pairs. Single ions are unlikely due to the large dissociation energy of the ion pair. Since the substrate is crystalline, one can describe any deviations of the molecular environment, i.e., the morphology of the underlying KCl substrate from the ideal one, entirely by a specific spatial distribution of these defects. Energetically most likely are defects located at the step edge that lead to "rough" and/or kinked step edges which hence differ from ideal straight step edges. Such defects exist due to entropic and kinetic reasons. They are indeed observed in STM images [17].

In principle, the KCl ion pairs interact with the molecule by Coulomb and van der Waals (vdW) interactions. The defects which we consider here must be located at some distance to the molecule because otherwise the concept of a defined adsorption site would be meaningless in contradiction to the experimental finding of well defined lines in the FL spectra of the ensemble as reported above. In addition, our profile interpretation below consistently yields a significant defect-free zone around the PTCDA molecules. Because of the decrease of the Coulomb and vdW interactions with distance the interactions are relatively small and their contribution to the  $S_0$  and  $S_1$  states can be considered in a perturbative manner by adding the interaction energies between the molecule and the defects (far-field effect) to the energies of the unperturbed states. This approach is also justified by the localization of the  $S_1$  and  $S_0$  states on the molecule. In principle, one may also consider the possibility that a second molecule acts as a perturber/defect. However, this contribution is less relevant here because of the very small coverage of the molecules.

### F. Dipole-dipole interaction between PTCDA and KCl

Because the molecule is uncharged, the relevant electrostatic interactions with KCl ion pairs will be given by dipole-dipole interactions. The KCl ion pairs act as electrostatic dipoles with their dipole axes being about parallel to the surface plane. In the following, we denote the electrostatic dipole of a KCl defect by  $\vec{p}_{\text{KCl}}$ . The vdW interaction between the molecule and the KCl is less relevant for the profile broadening. First, and principally, because it is less effective due to its scaling with a higher power law ( $r^{-6}$ ) compared to the dipole-dipole interaction ( $r^{-3}$ ). Secondly, contrary to the dipole-dipole interaction, the vdW interaction is always attractive. As a consequence, for vdW interactions the line broadening due to statistical defects is correlated with a shift of the line position to lower energies [31]. When we compare spectra from different experiments, which yielded slightly different surface and step morphologies due to small variations in the sample preparation, this effect is not observed. Hence, we conclude that the vdW interactions with defects is not relevant here and neglect it.

Important for the dipole-dipole interaction is that the adsorption complex of the PTCDA molecule at a step site exhibits a reduced symmetry ( $C_1$ ) with respect to that of a molecule adsorbed on a terrace ( $C_{2v}$ ). This has been found both experimentally from the appearance of additional vibrational modes and from DFT calculations of the adsorbed molecule [21]. A detailed representation of the structure of the adsorption complex at the step edge is given in Fig. 1 of Ref. [21]. As a consequence, the molecule at a step site

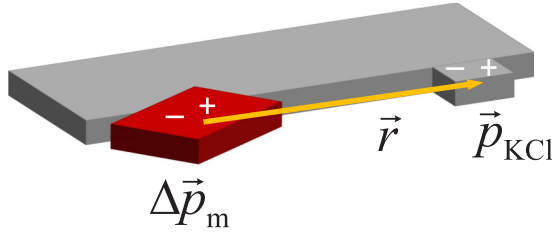


FIG. 4. Schematic drawing of the dipole-dipole interaction of the PTCDA molecule ( $\Delta\vec{p}_m$ ) and a KCl dipole at the step edge.

exhibits a nonzero electrostatic dipole moment  $\vec{p}_m$ , which is mainly oriented in the direction of its long axis and parallel to the plane of the surface. The relevant effect is that the symmetry between the two anhydride groups of the PTCDA is lost. One is oriented towards the upper terrace and thus protrudes into the step edge, whereas the other points towards the lower terrace. We note that, different from the molecules at the step edge, the adsorption complex of molecules adsorbed on terraces exhibits a zero dipole moment in the plane of the surface due to symmetry reasons.

For sufficiently large molecule-to-defect distances the interaction of the molecule and the defects ( $\vec{p}_{\text{KCl}}$ ) can be described by the interaction between two electrostatic point dipoles which yields an interaction energy  $\Delta E$ :

$$\Delta E = \frac{1}{4\pi\epsilon_0} \left( \frac{\vec{p}_m \cdot \vec{p}_{\text{KCl}}}{r^3} - \frac{3(\vec{p}_m \cdot \vec{r})(\vec{p}_{\text{KCl}} \cdot \vec{r})}{r^5} \right). \quad (2)$$

Here,  $\vec{r}$  denotes the vector from the molecule to the defect dipole.  $\epsilon_0$  is the dielectric constant of the vacuum. The equation is true for both the  $S_1$  and the  $S_0$  state; the dipole moment  $\vec{p}_m$  of the molecule differs for the  $S_1$  and  $S_0$  states. If  $\vec{p}_m$  is replaced by the difference of the dipole moments of the two states  $\Delta\vec{p}_m = \vec{p}_m^{S_1} - \vec{p}_m^{S_0}$ , Eq. (2) directly yields the differential shift  $\Delta\nu = \Delta E/(hc)$  of the line position [given by Eq. (1)] due to the specific defect. The situation is schematically illustrated in Fig. 4.

For a quantitative profile evaluation we need the value of  $\Delta\vec{p}_m$ . For this purpose we calculated the total electric dipole of the adsorption complex for both the  $S_0$  and the  $S_1$  state by DFT. The calculations were performed with GAUSSIAN09 [33]. The excited state was calculated with the time-dependent density functional theory employing the CAM-B3LYP functional [34,35] and 6-311G\*\* basis sets for H, C, and O. K and Cl were described with standard basis sets from the CRYSTAL website [36–39]. More details of the computational setup can be found in Ref. [40].

The calculated cluster models had a size of about  $3 \times 3$  KCl lattice constants in the plane of the surface and comprised a few KCl layers in the direction normal to the surface. Due to polarized edges of the calculated clusters the electric dipoles of the  $S_0$  and  $S_1$  states of the entire clusters themselves are not meaningful. However, these charges that are located at the outer edges of the calculated clusters cancel for  $\Delta\vec{p}_m = \vec{p}_m^{S_1} - \vec{p}_m^{S_0}$  due to the localized nature of the excitation. Hence, the calculated values of  $\Delta\vec{p}_m$  are meaningful.

The electrical dipole of the KCl ion pair which constitutes the defect was approximated by the distance between the

TABLE I. Overview on the parameters used for the description of the inhomogeneous line profile. For the calculation of  $\beta$  according to Eq. (6) we used the average of the  $|\Delta\vec{p}_m|$  values for the two sites. For further details see text.

Deep vacancy site	$ \Delta\vec{p}_m $	$0.366e \text{ \AA}$	1.76 D
Deep vacancy site + 1	$ \Delta\vec{p}_m $	$0.314e \text{ \AA}$	1.51 D
KCl defect	$ \vec{p}_{\text{KCl}} $	$3.15e \text{ \AA}$	15.1 D
	$\beta$	$30.8 \text{ \AA}^3 \text{ eV}$	

ion cores ( $0.5a_{\text{KCl}}$ ) times the elementary charge. The relevant parameters are summarized in Table I.

### G. Application of the stochastic theory to two dimensions

As noted above, for optical transitions of molecules the stochastic line broadening due to dipole-dipole interactions has been considered for the 3D case in detail by Kador [31]. He assumed uncorrelated and identical defects with a constant density. In addition, for mathematical purposes, a radial orientation of the dipole moment of the defects with respect to the molecule was used ( $\vec{p}_{\text{KCl}}$  parallel to  $\vec{r}$ ; cf. Fig. 4). As a consequence, all azimuthal orientations of the defects with respect to the molecule occur with the same probability. In addition, the probability of the presence of a defect with respect to the molecule regarding the distance and orientation exhibits an inversion symmetry. For this symmetry, the dipole-dipole coupling [cf. Eq. (2)] implies that  $\Delta E(\vec{r}) = -\Delta E(-\vec{r})$ . In combination with the above noted inversion symmetry of the defect probability this causes the distribution of the pairwise interaction energies to be centered at zero. Thus, the described scenario does not lead to a shift of the line, but only to broadening.

In our case, we have to consider defects given by additional KCl dipoles and defects due to KCl vacancy dipoles. For identical values of  $\vec{r}$  and identical orientations of the dipoles, the respective interactions differ only in sign, i.e.,  $\Delta E_{\text{additional dipole}}(\vec{r}) = -\Delta E_{\text{vacancy dipole}}(\vec{r})$  holds. Because of the above noted inversion symmetry of the probability of the additional defects and the described symmetry of the dipole-dipole coupling the distribution of the resulting interaction energies stays the same when additional dipoles are replaced by vacancy dipoles. This is of course valid only as long as the additional and vacancy dipoles are subject to the same type of probabilities. In that case, the distributions of resulting interaction energies are the same. Conclusively, we do not have to consider both types of defects separately, but can describe them in common by one density of defects.

All of these assumptions, in particular the neglect of spatial correlations between defects, are of course worth discussion for the present situation of a crystalline system, which restricts the orientations of the dipoles by the presence of the crystal lattice. In addition, the preferential location of the defects along the step edges may imply spatial correlations between the defects. However, these additional aspects are difficult to describe by quantitative models. For the present analysis we thus postpone them. This is also a pragmatic approach because we were primarily interested in the general aspects of the

line shape interpretation for this two-dimensional system on a surface.

For dipole-dipole coupling Kador found that the line shape is of Gaussian type only if the defect density exceeds a critical value, otherwise the line profile exhibits a Lorentzian shape [31]. As mentioned by Kador, this phenomenon can be understood by the central limit theorem that is only valid for large defect densities. Evidently, a similar situation of low defect concentrations holds for the present system, too, because, as said above and shown below in Fig. 5(c), a fit of the experimental profile by Gaussian line profiles fails, whereas a fit by Lorentzian profiles is successful. However, when the calculation given by Kador for three dimensions (3D) is transferred to the present two-dimensional (2D) situation, slightly different profile shapes are obtained due to the reduced dimensionality, which we need to take into consideration.

Quite generally, for sufficiently low defect densities the line shape can be expressed by a symmetric Lévy distribution [41] which is defined generally via a Fourier transformation:

$$I(\nu) = \frac{1}{\pi} \int_0^{\infty} dx \cos(\nu x) \exp[-(\kappa x)^{\gamma}]. \quad (3)$$

Here,  $\nu$  denotes the energy with respect to the maximum of the line profile, and  $x$  is the Fourier counterpart of the energy. The scaling parameter  $\kappa$  determines the line width. It depends on the defect density and the strength of the interaction between the molecule and the defects. The parameter  $\gamma$  determines the line shape. In general it depends on the decay of the interaction with distance; here we consider the dipole-dipole interaction only. For  $\gamma = 2$  and  $\gamma = 1$ , a Gaussian and a Lorentzian line shape are obtained, respectively. As reported by Kador for 3D [31],  $\gamma$  changes from 1 to 2 when the defect density is increased. The Lorentzian line shape ( $\gamma = 1$ ) is thus only obtained in the limit of low defect concentrations. To be more precise, the defect density  $\varrho$  is measured versus the reciprocal volume of a defect-free zone around the molecule. This zone can be also understood a “near field” of the molecule that is free of defects. The existence of a defect-free zone is required, since otherwise the definition of the specific molecular site (and its corresponding transition) would become meaningless and contradict the experimental observation of well defined transition energies. If the defect-free volume is denoted by  $R_c^3$ , the criterion for a low defect concentration in 3D is

$$\varrho_{3D} R_c^3 \ll 1. \quad (4)$$

Finally, the dimensionality of the system also has an impact on  $\gamma$ . For 2D, our calculation yields  $\gamma = 2/3$  in the limit of low defect concentrations. Accordingly, the 2D line profile exhibits heavier wings which fall off less rapidly  $I(\nu) \sim 1/\nu^{1+\kappa}$  with respect to the wings of a Lorentzian profile, and the maximum has a sharper cusp.

In order to test whether such a predicted line profile fits the experimental profile, we have performed a fit to the experimental data by Lévy distributions given by Eq. (3) using the appropriate exponent  $\gamma = 2/3$  of a 2D system. In the following, we use the term Lévy distribution to refer to profiles with exponents  $\gamma$  different to those of the Gaussian or Lorentzian cases. The achieved fit is shown in Fig. 5(b). As explained

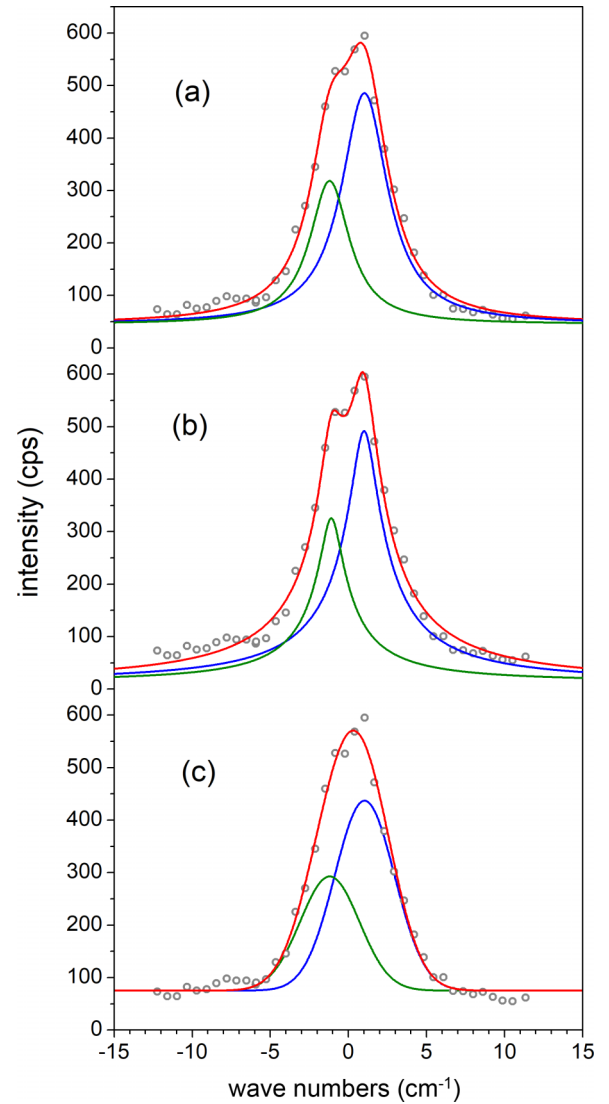


FIG. 5. Fit of the FLE spectrum from Fig. 1(a) according to Eq. (3) by (a) two Lorentzians ( $\gamma = 1$ ), (b) by two Lévy distributions ( $\gamma = 2/3$ ), and two Gaussians ( $\gamma = 2$ ). A constant background was fitted in addition. The scaling parameters  $\kappa$  were 1.56 and 1.81  $\text{cm}^{-1}$  in (a), 2.77 and 3.29  $\text{cm}^{-1}$  in (b), and 1.36 and 1.34  $\text{cm}^{-1}$  in (c). For the Lorentzian  $\kappa = \frac{1}{2}$  FWHM, for the Lévy distribution  $\kappa \approx$  FWHM, and for the Gaussian  $\kappa = (4\sqrt{\ln 2})^{-1}$  FWHM  $\approx$  0.300 FWHM holds. Note the less good fit of the top of the profile and of the profile wing on the high energy side between 5 and 10  $\text{cm}^{-1}$  for the two Gaussians (c). Contrary to the fits in (a) and (b), the positions of the two Gaussians had to be fixed, as they merged otherwise for the benefit of a better fit of the profile wings.

above, the presence of two energetically very similar sites requires a fit by a sum of two distributions shifted against each other by a small energy of 2.2  $\text{cm}^{-1}$ . The fit by two Lévy distributions is successful and, in particular, the sharp maximum at the top of the experimental profile is well reproduced. A fit by the two Lorentzians ( $\gamma = 1$ ) is shown in Fig. 5(a) for direct comparison. This fit is of slightly better quality than the former concerning the reproduction of the wings of the experimental spectrum at about +5 and -5  $\text{cm}^{-1}$ . However, this subtle difference is at the limit of the signal-to-noise



ratio. We also show a fit by two Gaussians in Fig. 5(c) for comparison. This fit, in particular, does not well describe the profile wing on the high energy side. Our conclusion from Fig. 5 is thus that the fit by two Lévy distributions is also fully compatible with the experimental data, although, at present, the quality of the data prevents a firm determination of  $\gamma$  and thus a clear discrimination against the fit by two Lorentzians. For further quantitative evaluation we use the equations which are valid for the 2D case, i.e., for the Lévy distribution with  $\gamma = 2/3$ .

#### H. Quantitative evaluation of the line shape

We calculated the defect density  $\varrho$  from the widths of the line profiles. In the 3D case, the following relation of  $\kappa$  and the defect density  $\varrho_{3D}$  was obtained [Ref. [31], Eq. (15)]:

$$\kappa = \frac{\pi^2}{3} \varrho_{3D} \beta \approx 3.29 \varrho_{3D} \beta, \quad (5)$$

where we use the abbreviation

$$\beta = \frac{2 |\Delta \vec{p}_m| |\vec{p}_{KCl}|}{4\pi \epsilon_0 h c}. \quad (6)$$

For 2D the analogous relation for the scaling parameter is obtained as [ $\Gamma(\frac{1}{6}) \approx 5.57$ ]:

$$\kappa = \left( \frac{3\pi^{3/2}}{\Gamma(\frac{1}{6})} \varrho_{2D} \right)^{3/2} \beta \approx 5.20 \varrho_{2D}^{3/2} \beta. \quad (7)$$

For the details we refer to the Appendix. Numerically, we derived that  $\kappa$  agrees with the FWHM of the profile within a few percent. We calculated  $\varrho_{2D}$  from  $\kappa$  via Eq. (7). Here we fitted the experimental data by a sum of two Lévy distributions and obtained two very similar values of  $\kappa$  for the two distributions (see caption of Fig. 5). This indicates that the defect densities that are derived for both types of adsorption sites are very similar, which is expected and plausible. For the further calculation, we used the average of the two  $\kappa$  values. For  $\bar{\kappa} = 3.0 \text{ cm}^{-1}$ , we obtained  $\varrho_{2D} = 1.75 \times 10^{-4} \text{ \AA}^{-2}$  from Eq. (7). Normalization of  $\varrho_{2D}$  to the area of one KCl dipole ( $0.5 \times a_{KCl}^2 = 19.8 \text{ \AA}^2$ ) yields a defect density of 0.35%. This corresponds to about one defect per  $17 \times 17$  KCl dipoles on the surface. The footprint of the PTCDA molecule ( $120 \text{ \AA}^2$ ) covers an area of about 6 KCl dipoles. This value is by a factor of about 50 smaller than the reciprocal defect density. The obtained value of  $\varrho_{2D}$  thus appears reasonable.

Finally, we discuss the criterion (4), which reads  $\varrho_{2D} R_c^2 \ll 1$  in 2D. It has to be fulfilled because otherwise a Gaussian line shape is expected. If we estimate the size of the defect-free zone ( $R_c^2$ ) around the PTCDA molecule by the footprint of the molecule, we find  $\varrho R_c^2 \approx 1/50$ . Hence, the criterion  $\varrho_{2D} R_c^2 \ll 1$  is fulfilled and indicates that our model is consistent.

In summary, we have presented a quantitative interpretation of the inhomogeneous line shape of PTCDA molecules adsorbed at steps on a KCl(100) surface. In view of the simplicity of the model and its noted shortcomings, e.g., the neglect of spatial correlations between the defects, the derived defect density should be not overinterpreted. We suggest that this type of line shape interpretation is valid for optical spectra of similar molecules on other ionic substrates, too. In addition, the given 2D theoretical description may also be useful for

the analysis of inhomogeneous line broadening encountered in other surface related spectroscopies, i.e., photoemission.

#### IV. CONCLUSIONS

In conclusion, we measured single molecule excitation spectra of PTCDA adsorbed on the KCl(100) surface. The ZPL exhibits a Lorentzian shape corresponding to a dephasing time of 0.70 ns. We can conclude that the lifetime of the adsorbed molecule is reduced by a factor of at most 15 with respect to the FL lifetime  $T_1 = 5.5$  ns of the molecule in ultracold He droplets. This value hence sets an upper limit for the effect of the KCl surface on the FL lifetime which could be envisaged due to surface-induced molecular distortions related to the adsorption process. FL spectra of this, and similar molecules, on surfaces recorded by STM-LE need to be discussed on this background. Our results indicate that line broadening may be related to the STM-LE process itself or, in the case of very thin films, the underlying metal substrate [23]. The inhomogeneous line profile of the ensemble is also of Lorentzian type and given by the statistical interaction with surface defects, i.e., misplaced KCl ion pairs. The density of these surface defects is small, because for higher densities of defects the theory that successfully describes the measured line profile would predict a change to a Gaussian shape.

#### ACKNOWLEDGMENTS

We thank A. Eisfeld, R. Höfer, L. Kador, and F. Stienkemeier for helpful discussions. This project was supported by the Deutsche Forschungsgemeinschaft (DFG) under Grant No. SO407/8-1.

#### APPENDIX

We report how Eq. (7) is derived for the 2D analogous to the derivation given by Kador for the 3D case [31]. According to [31], Eq. (7), the line shape is given by

$$I(\nu) = \frac{1}{2\pi} \int_{-\infty}^{+\infty} dx e^{i\nu x} e^{-J(x)}, \quad (A1)$$

where  $J(x)$  is given as

$$J(x) = \varrho \int_{(V)} d\mathbf{R} g(\mathbf{R}) (1 - e^{i\tilde{\nu}(\mathbf{R}) \cdot x}). \quad (A2)$$

Hereby  $\varrho$  denotes the number density of the defects,  $g(\mathbf{R})$  the distribution function of the defects, and  $\tilde{\nu}(\mathbf{R})$  the contribution to the energetic shift by the defect. Following Kador and using

$$g(\mathbf{R}) = \begin{cases} 1 & \text{for } R \geq R_c \\ 0 & \text{for } R < R_c \end{cases}$$

and

$$\tilde{\nu}(\mathbf{R}) = -\beta \cos \vartheta / R^3, \quad (A3)$$

[for  $\beta$  see Eq. (6) in the main text] one obtains from Eq. (A2)

$$J(x) = 2\pi\varrho \int_{R=R_c}^{\infty} \int_{\vartheta=0}^{\pi} R^2 dR \sin \vartheta d\vartheta \{1 - e^{i\beta(\cos \vartheta / R^3)x}\}. \quad (A4)$$

For the 2D case this modifies to

$$J(x) = \varrho \int_{\varphi=0}^{2\pi} d\varphi \int_{R=R_c}^{\infty} R dR \{1 - e^{i\beta(\cos\varphi/R^3)x}\}. \quad (\text{A5})$$

Using

$$\int_0^{2\pi} e^{i\alpha \cos x} dx = 2\pi J_0(\alpha), \quad (\text{A6})$$

where  $J_0$  denotes the Bessel function and because of  $J_0(x) = J_0(-x)$ , Eq. (A5) yields

$$J(x) = 2\pi \varrho \int_{R=R_c}^{\infty} R dR \left\{1 - J_0\left(\frac{\beta|x|}{R^3}\right)\right\}. \quad (\text{A7})$$

Substituting  $u = \frac{\beta|x|}{R^3}$  gives

$$J(x) = 2\pi \frac{1}{3} (\beta|x|)^{2/3} \varrho \int_0^{\beta|x|/R_c^3} \frac{1}{u^{5/3}} \{1 - J_0(u)\} du. \quad (\text{A8})$$

We further consider the case of low defect concentration, i.e.,  $|x| \rightarrow \pm\infty$  or  $\beta|x| \gg R_c$ , respectively. Hence we can approximate

$$J(x) \approx 2\pi \frac{1}{3} (\beta|x|)^{2/3} \varrho \int_0^{\infty} \frac{1}{u^{5/3}} \{1 - J_0(u)\} du \quad (\text{A9})$$

$$= 2\pi \frac{1}{3} (\beta|x|)^{2/3} \varrho \frac{9\sqrt{\pi}}{2\Gamma(\frac{1}{6})} \quad (\text{A10})$$

$$\approx 2\pi \frac{1}{3} (\beta|x|)^{2/3} \varrho 1.433 \quad (\text{A11})$$

$$= 2.997(\beta|x|)^{2/3} \varrho. \quad (\text{A12})$$

Hence, we obtain the symmetric line profile according to Eq. (A1) as

$$I(v) = \frac{1}{\pi} \int_0^{+\infty} dx \cos(vx) \exp[-(\kappa x)^{2/3}], \quad (\text{A13})$$

whereby the parameter  $\kappa$  is given by  $\kappa = (2.997\beta^{2/3}\varrho)^{3/2} = 5.20\varrho^{3/2}\beta$ .

- 
- [1] W. E. Moerner, and L. Kador, *Phys. Rev. Lett.* **62**, 2535 (1989).
- [2] M. Orrit and J. Bernard, *Phys. Rev. Lett.* **65**, 2716 (1990).
- [3] W. P. Ambrose, T. Basché, and W. E. Moerner, *J. Chem. Phys.* **95**, 7150 (1991).
- [4] T. Basché, W. P. Ambrose, and W. E. Moerner, *J. Opt. Soc. Am. B* **9**, 829 (1992).
- [5] L. Fleury, A. Zumbusch, M. Orrit, R. Brown, and J. Bernard, *J. Lumin.* **56**, 15 (1993).
- [6] P. Tchénio, A. B. Myers, and W. E. Moerner, *J. Lumin.* **56**, 1 (1993).
- [7] M. Orrit, J. Bernard, A. Zumbusch, and R. I. Personov, *Chem. Phys. Lett.* **196**, 595 (1992).
- [8] X. H. Qiu, G. V. Nazin, and W. Ho, *Science* **299**, 542 (2003).
- [9] B. Doppagne, M. C. Chong, E. Lorchat, S. Berciaud, M. Romeo, H. Bulou, A. Boeglin, F. Scheurer, and G. Schull, *Phys. Rev. Lett.* **118**, 127401 (2017).
- [10] C. Chen, P. Chu, C. A. Bobisch, D. L. Mills, and W. Ho, *Phys. Rev. Lett.* **105**, 217402 (2010).
- [11] C. Chen, C. A. Bobisch, and W. Ho, *Science* **325**, 981 (2009).
- [12] M. C. Chong, G. Reeht, H. Bulou, A. Boeglin, F. Scheurer, F. Mathevet, and G. Schull, *Phys. Rev. Lett.* **116**, 036802 (2016).
- [13] X. L. Guo, Z. C. Dong, A. S. Trifonov, K. Miki, K. Kimura, and S. Mashiko, *Appl. Surf. Sci.* **241**, 28 (2005).
- [14] Y. Luo, G. Chen, Y. Zhang, L. Zhang, Y. Yu, F. Kong, X. Tian, Y. Zhang, C. Shan, Y. Luo, J. Yang, V. Sandoghdar, Z. Dong, and J. G. Hou, *Phys. Rev. Lett.* **122**, 233901 (2019).
- [15] H. Imada, K. Miwa, M. Imai-Imada, S. Kawahara, K. Kimura, and Y. Kim, *Phys. Rev. Lett.* **119**, 013901 (2017).
- [16] K. Kimura, K. Miwa, H. Imada, M. Imai-Imada, S. Kawahara, J. Takeya, M. Kawai, M. Galperin, and Y. Kim, *Nature (London)* **570**, 210 (2019).
- [17] Q. Guo, A. Paulheim, M. Sokolowski, H. Aldahhak, E. Rauls, and W. G. Schmidt, *J. Phys. Chem. C* **118**, 29911 (2014).
- [18] M. Müller, A. Paulheim, C. Marquardt, and M. Sokolowski, *J. Chem. Phys.* **138**, 064703 (2013).
- [19] A. Paulheim, M. Müller, C. Marquardt, and M. Sokolowski, *Phys. Chem. Chem. Phys.* **15**, 4906 (2013).
- [20] A. Paulheim, C. Marquardt, H. Aldahhak, E. Rauls, W. G. Schmidt, and M. Sokolowski, *J. Phys. Chem. C* **120**, 11926 (2016).
- [21] A. Paulheim, C. Marquardt, M. Sokolowski, M. Hochheim, T. Bredow, H. Aldahhak, E. Rauls, and W. G. Schmidt, *Phys. Chem. Chem. Phys.* **18**, 32891 (2016).
- [22] M. Müller, J. Ikonov, and M. Sokolowski, *Surf. Sci.* **605**, 1090 (2011).
- [23] K. Stallberg, A. Namgalies, and U. Höfer, *Phys. Rev. B* **99**, 125410 (2019).
- [24] C. Marquardt, A. Paulheim, N. Rohbohm, R. Merkel, and M. Sokolowski, *Rev. Sci. Instrum.* **88**, 083702 (2017).
- [25] W. E. Moerner and T. P. Carter, *Phys. Rev. Lett.* **59**, 2705 (1987).
- [26] S. Kummer, S. Mais, and T. Basché, *J. Phys. Chem.* **99**, 17078 (1995).
- [27] O. Bünermann, *Spektroskopie von Alkali- und Erdalkaliatomen, -molekülen, Alkaliclustern und Komplexen Organischer Moleküle auf Heliumnanotropfchen*, Ph.D. thesis, University of Bielefeld, 2006.
- [28] T. Plakhotnik, W. E. Moerner, V. Palm, and U. P. Wild, *Opt. Commun.* **114**, 83 (1995).
- [29] W. E. Moerner, T. Plakhotnik, T. Irngartinger, M. Croci, V. Palm, and U. P. Wild, *J. Phys. Chem.* **98**, 7382 (1994).
- [30] A. Stoneham, *Rev. Mod. Phys.* **41**, 82 (1969).
- [31] L. Kador, *J. Chem. Phys.* **95**, 5574 (1991).
- [32] S. H. Simon, V. Dobrosavljevic, and R. M. Strat, *J. Chem. Phys.* **93**, 2640 (1990).
- [33] M. J. Frisch, G. W. Trucks, H. B. Schlegel, G. E. Scuseria, M. A. Robb, J. R. Cheeseman, G. Scalmani, V. Barone, B. Mennucci, G. A. Petersson *et al.*, *Gaussian 09, Revision D.01* (Gaussian Inc., Wallingford, CT, 2009).

- [34] T. Yanai, P. T. David, and C. H. Nicholas, *Chem. Phys. Lett.* **393**, 51 (2004).
- [35] M. J. G. Peach, P. Benfield, T. Helgaker, and D. J. Tozer, *J. Chem. Phys.* **128**, 044118 (2008).
- [36] R. Dovesi, C. Roetti, C. Freyria-Fava, M. Prencipe, and V. Saunders, *Chem. Phys.* **156**, 11 (1991).
- [37] B. Civalleri, A. M. Ferrari, M. Llunell, R. Orlando, M. M erawa, and P. Ugliengo, *Chem. Mater.* **15**, 3996 (2003).
- [38] E. Apra, M. Causa, M. Prencipe, R. Dovesi, and V. R. Saunders, *J. Phys.: Condens. Matter* **5**, 2969 (1993).
- [39] R. Krishnan, J. S. Binkley, R. Seeger, and J. A. Pople, *J. Chem. Phys.* **72**, 650 (1980).
- [40] M. Hochheim, A. Paulheim, M. Sokolowski, and T. Bredow, *J. Phys. Chem. C* **120**, 24240 (2016).
- [41] A. Eisfeld, S. M. Vlaming, V. A. Malyshev, and J. Knoester, *Phys. Rev. Lett.* **105**, 137402 (2010).